Received: 18 July 2022 | Revised: 21 September 2022 | Accepted: 24 September 2022

DOI: 10.1002/ardp.202200383

FULL PAPER

ARCH PHARM DPhG
Archiv der Pharmazie

Structure-guided identification of a selective sulfonamide-based inhibitor targeting the human carbonic anhydrase VA isoform

Laura De Luca[1] | Andrea Angeli[2] | Federico Ricci[1] | Claudiu T. Supuran[2] | Rosaria Gitto[1]

[1]Chibiofaram Department, University of Messina, Messina, Italy

[2]Neurofarba Department, University of Florence, Florence, Italy

Correspondence
Rosaria Gitto, Chibiofaram Department, University of Messina, Viale Ferdinando Stagno D'Alcontres, Messina 31, I-98166, Italy.
Email: rosaria.gitto@unime.it

Claudiu T. Supuran, Neurofarba Department, University of Florence, Via U. Schiff 6, Florence I-50019, Italy.
Email: claudiu.supuran@unifi.it

Funding information
Ministero dell'Università e della Ricerca, Grant/Award Number: PRIN_201744BN5T_002

Abstract

In recent years, multistep hybrid computational protocols have attracted attention for their application in the drug discovery of enzyme inhibitors. So far, there are large collections of human carbonic anhydrase (hCA) inhibitors, but only a few of them selectively inhibit the mitochondrial isoforms hCA VA and VB as potential therapeutics in obesity treatment. Most sulfonamide-based inhibitors show poor selectivity for inhibiting isoforms of therapeutic interest over ubiquitous hCA I and hCA II. Herein, we propose a combination of ligand- and structure-based approaches to generate pharmacophore models for hCA VA inhibitors. Then, we performed a virtual screening (VS) campaign on a database of commercially available sulfonamides. Finally, the in silico screening followed by docking studies suggested several "hit compounds" that demonstrated to inhibit hCA VA at a low nanomolar concentration in a stopped-flow CO_2 hydrase assay. Notably, the best candidate, 2-(3,4-dihydro-2*H*-quinolin-1-yl)-*N*-(4-sulfamoylphenyl)acetamide (code name VAME-**28**) proved to be a potent hCA VA inhibitor (K_i value of 54.8 nM) and a more selective agent over hCA II when compared to the reference compound topiramate.

KEYWORDS
carbonic anhydrase, docking studies, hCA VA, pharmacophore model, virtual screening

1 | INTRODUCTION

Both overweight and obesity are considered related to an abnormal fat accumulation in adipose tissue corresponding to a body mass index (BMI) ≥ 30 kg/m^2. Currently, obesity represents a global health problem for people belonging to different age groups that suffer from multi-system diseases, related to cardiovascular pathologies, dyslipidemia, type 2 diabetes, hepatic steatosis, and atherosclerosis. Frequently, obesity also demonstrates several comorbidities with distinct pathologies such as osteoarthritis, infertility, and cancer.

It has been clearly demonstrated that weight gain is closely linked to an imbalance of energy intake or energy expenditure. Based on this consideration, the most classical therapeutic strategy foresees a combination of healthy nutritional habits with administration of antiobesity drugs aimed to reduce food intake or nutrient absorption.[1] The most popular antiobesity agents are sympathomimetic

Laura De Luca and Andrea Angeli contributed equally to this study.

agents, $GABA_A$ receptor activators, pancreatic lipase inhibitors, $5H_{T2C}$ receptor agonists, opioid receptor antagonists, dopamine–norepinephrine reuptake inhibitors, and glucagon-like peptide-1 (GLP-1) receptor agonists.[2,3] Unfortunately, these agents are not often able to fight the obesity in absence of undesired effects.[4] Therefore, the development of newer agents for the most innovative and attractive drug targets might be useful to address a combination therapy with well-established antiobesity drugs.[5]

Some studies have identified the deregulation of mitochondrial enzymes as a crucial event in metabolic disorders. Specifically, the acid fatty metabolism, as well as the glucose homeostasis, are regulated by the carbonic anhydrase isoform CA VA.[6–9] It is well known that human carbonic anhydrases (hCA, EC 4.2.1.1) are metalloproteins catalyzing the CO_2 hydration into bicarbonate and proton in various organisms. Therefore, CAs are involved in many physio/pathological pathways.[10] CAs are classified in 16 different isoforms displaying a high degree of similarity and are distributed in distinct organs, tissues, and cells; specifically, hCA I-III, hCA VII and hCA XIII are cytosolic, whereas hCA IV, hCA IX, hCA XII, hCA XIV, and hCA XV are membrane-bound isoforms; notably, hCA VA and hCA VB isoforms are mitochondrial enzymes and hCA VI is a secreted isoform. hCAs belong to the α-class, which is characterized by the presence of zinc ion (zinc II) coordinated by three histidine residues in the catalytic cavity as detailed by X-ray crystallographic data.

There is evidence that several small molecules could target the mitochondrial isoforms hCA VA and VB, which seem to be involved in lipogenesis and gluconeogenesis, thus corroborating the proof-of-concept of CA-mediated antiobesity effects of the CA inhibitors topiramate (TPM) and zonisamide (ZNS) (Figure 1).[6,7]

TPM is a sulfamate derivative able to modulate voltage-gated sodium channels and improve $GABA_A$ receptor activity; TPM also interacts with AMPA/kainate glutamate receptors as well as voltage-gated R-type calcium channels. Interestingly, the TPM-mediated inhibition of hCA might be related to its antiobesity effects.[11] Recently, TPM is employed in adjunctive therapy for weight management in association with the active molecule phentermine (QNEXA) for long-term treatment of obesity.[12] It was suggested that TPM is also capable to reduce food intake by modulation of voltage-gated ion channels, improvement of activity of γ-aminobutyric acid (GABA) receptor, and inhibition of ionotropic glutamate receptors.

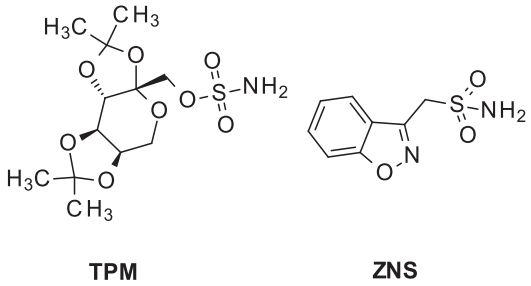

FIGURE 1 Chemical structures of topiramate (TPM) and zonisamide (ZNS)

Like the combination of TPM/phentermine, the sulfonamide-based CA-inhibitor ZNS also entered clinical trial in combination with the drug bupropion (EMPATIC)[13]; however, the associated mechanism of antiobesity activity of EMPATIC is a selective serotonin-receptor agonism and dopamine and norepinephrine reuptake inhibitory activity, while the involvement of CA inhibition has not been clearly demonstrated.[13]

While the attractiveness of targeting hCA II, hCA VII, hCA IX, and hCA XII has been clear from a therapeutic perspective, the inhibition of CA VA isoform still constitutes only a plausible mechanism of CA-mediated pharmacological effects of TPM and ZNS as antiobesity agents.[7–9] Therefore, the identification of newer small molecules binding CA VA/VB isoforms with high affinity and selectivity might represent a challenging objective to improve our knowledge of antiobesity therapeutic potential of CA-inhibitors for further theranostic applications.

Co-crystal structures of sulfonamide-based hCA inhibitors (hCAIs) in complexes with the most popular hCA isoforms revealed that the knowledge of the active site of targeted CAs is crucial to accomplish the identification of selective hCAIs.[14–19] Structural determination confirmed that there are common areas in the catalytic sites as well as distinct regions in the hCA cavity regulating the catalytic cycle of CO_2 hydration. It was observed that the key chemical feature of hCAI corresponds to the sulfonamide/sulfamate moiety able to coordinate the zinc ion located in the deep region of the CA cavity (see Figure 2).[20,21] Then, additional crucial interactions are made by hydrophobic/hydrophilic chemical fragments that might establish crucial polar or hydrophobic interactions with residues paving the two walls of the CA cavity in the middle and top areas, in which there are distinct amino acids sketching the different shape of each isoform. While the main interactions of hCA II inhibitors are well described through large numbers of crystal data, little information is available for the true crucial residues and relevant contacts controlling hCA VA affinity/selectivity of hCAIs.[22–24]

In this study, we sought to exploit a multistep computational approach to discover new chemical entities based on the sulfonamide binding motif as a well-known key feature to binding the hCA VA catalytic site. In the present study, we combined ligand-based (LB) and structure-based (SB) virtual screening (VS) methods, thus leading to the identification of plausible pharmacophoric hypotheses for hCA VA inhibition, as a result, we were able to screen three-dimensional library of compounds available on a commercial database. The outcomes of this in silico screening campaign provided a set of hit compounds that were assayed to test their ability to inhibit hCA VA in comparison with other druggable hCAs.

2 | RESULTS AND DISCUSSION

To date no crystal structures are available for hCA V, thus hampering a classical SB approach to develop new ligands; therefore, an unconventional multistage computational process was considered necessary to reinforce the success of our VS strategy. Consequently,

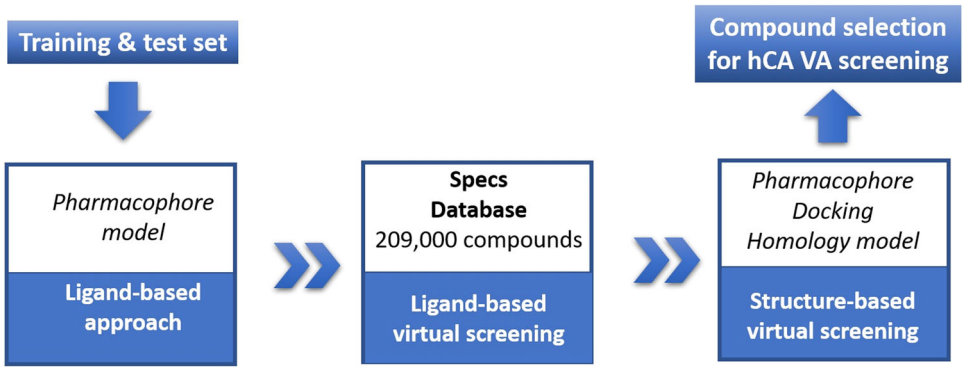

FIGURE 2 Overview of the applied computational strategy to select human carbonic anhydrase (hCA) VA sulfonamide-based inhibitors

our drug discovery approach employed a VS procedure that was based on the integration of LB and SB protocols. In more detail, starting from a collection of CA V inhibitors and the crystal structure of murine CA V isoform in complex with the well-known CA inhibitor acetazolamide (AAZ) we exploited the synergy between the LBVS and SBVS to improve the performance of the in silico screening to a large chemical database of compounds bearing the RSO_2NH_2 fragment. To augment the quality of a tailored compound library, in our screening workflow several sequential filters (3D-ligand pharmacophore model, drug-likeness, 3D-structure pharmacophore model, docking on constructed homology models) were leveraged for triaging a large compound collection. The application of these filters expedited the identification of a small set of compounds suitable for in vitro testing, thus validating our VS cascade methodology. The flowchart of our hybrid strategy for identification of hCA VA inhibitors is depicted in Figure 2.

2.1 | Ligand-based virtual screening

2.1.1 | Pharmacophore model generation

In the first round of our study, we developed an LB pharmacophore model by LigandScout software,[25] thus searching the three-dimensional spatial arrangements of the most relevant features that are crucial for CA V inhibitory effects. Figure 3 displays the selected 16 active inhibitors, showing K_i < 150 nM a selectivity ratio > 1; they were collected from the literature[26–31] based on the well-established stopped-flow assay for characterizing CA inhibitors and according to their structural diversity. Despite these molecules belong to distinct chemical scaffolds, they share the $ArSO_2NH_2$ or $ArNHSO_2NH_2$ group as key fragment capable to establish profitable contacts near zinc atom within CA catalytic site. To generate the pharmacophore models, the data set of active ligands was distributed in two subsets of compounds displayed in Figure 3: (i) the training set (a) and (ii) test set (b) by using the clustering procedure. In detail, the clustering has been performed by switching the similarity measurement (Pharmacophore Alignment score or Pharmacophore RDF-code similarity) in each clustering run and scaling the cluster distance from 0.4 (default value) to 0.5. The other clustering parameters were left as

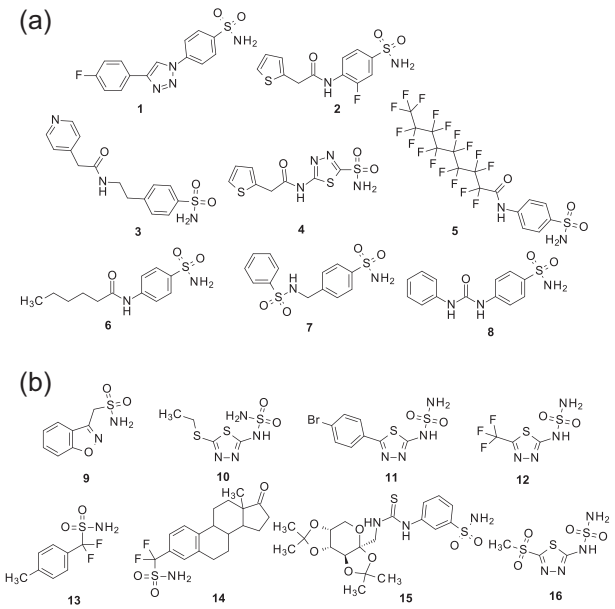

FIGURE 3 Chemical structures of 16 well-known human carbonic anhydrase (hCA) V inhibitors employed as the training set (a) and test set (b) retrieved from the literature[26–31]

default. For each clustering run, the biggest cluster was used as a training set, while the remaining clusters were used as tests; then a pharmacophore to validate via ROC curves was generated.

By employing the two data sets of 16 arylsulfonamides and sulfamides, 10 pharmacophore models were generated by LigandScout[25]; then, the pharmacophore hypothesis possessing the best score value was employed to perform further studies. In detail, the above-mentioned best pharmacophore model consisted of nine pharmacophoric features: three hydrogen bond acceptors (in red), two hydrogen bond donors (in green), three hydrophobic features (in yellow) and one aromatic ring feature (in blue) (see Figure 4).

For the selection and validation of the pharmacophore model in terms of discrimination power, we considered the enrichment factor (EF) as well as the area under the curve (AUC) of the receiver operating characteristic (ROC) curve. To better discriminate "active" and "inactive" compounds, three hydrophobic features and one

hydrogen bond acceptor feature were marked as optional features. Our model was validated by using 1707 total compounds distributed in two distinct datasets, (i) the first one containing 47 active molecules as sulfonamide-based CA inhibitors possessing a K_i-value < 10,000 nM; (ii) the second one was generated by means of the web tool DUD-E (http://dude.docking.org/) thus containing 1660 decoys.

Figure 4 draws the ROC plot, AUC, and EF factor values measured at 1%, 5%, 10%, and 100% for the best pharmacophore hypothesis that was used for these studies. As shown in Figure 3, the early enrichment (EF 1%) resulted in a value of 32.0 and an AUC value of 1.00; so the obtained pharmacophore model discriminated between active and inactive compounds. Overall, the model displayed a preference for active molecules having an AUC value of 0.82 and EF of 27.2.

2.1.2 | Database in silico screening

Once the pharmacophore model was derived, the VS on the "Specs Compound Library" of 209,000 compounds (specs database, https://www.specs.net) was carried out to identify new potential active CA V inhibitors by means of LigandScout software.[25] The in silico screening on the full database led to the identification of 1738 compounds; among them, we selected sulfonamide-based compounds possessing the following mandatory features: (i) a fit score value > 80; (ii) distinct chemical scaffolds. From this filtered database, the second session of our LB VS campaign provided a smaller series of 81 sulfonamides from the 1738 compounds that have previously matched the pharmacophore features; the full list of the potential 81 hits is reported in Supporting Information: Table S1.

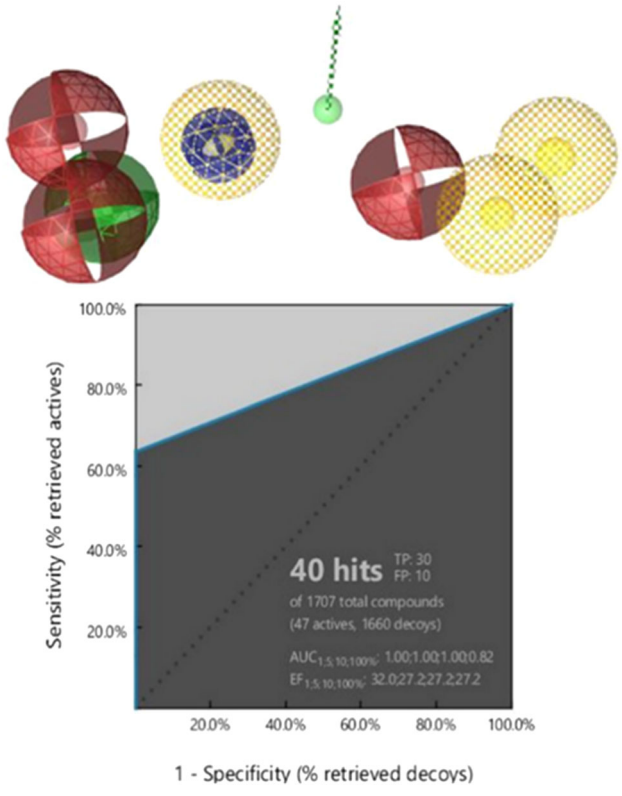

FIGURE 4 The LB pharmacophore model: three hydrogen bond acceptors (red); two hydrogen bond donors (green arrow); hydrophobic features (yellow) and one aromatic feature (blue circle). All optional features are not fully colored. Receiver operating characteristic validation curve for the pharmacophore model.

2.2 | Structure-based virtual screening

2.2.1 | Structure-based pharmacophore model

In the next stage, our efforts were addressed to further reduce the amount of 81 recovered sulfonamide-based compounds for biochemical assessment of CA VA inhibitory effects. Therefore, we chose to generate an additional SB pharmacophore model using LigandScout software.[25] We employed the crystal complex of murine mitochondrial CA V and AAZ (PDB code 1DMY)[32] as unique valuable candidate for enrichment of our pharmacophoric hypothesis. As depicted in Figure 5, the developed SB pharmacophore model consisted of five H-bond acceptor features matching three crucial residues T199, T200, and Y131.

To identify further plausible interactions within the CA V binding pocket, we analyzed the features from the apo-structure of the murine CA V (see Figure 6a) evaluating the possible interactions by using the "Create Apo Site Grids" as a tool that is implemented in LigandScout 4.4.[25] As a result, it was possible to highlight additional plausible features through the visual inspection of the co-crystallized inhibitor. Therefore, the refined pharmacophore model now consisted of six hydrophobic spheres, two positive ionizable, two aromatic rings, five H-bond acceptors, five H-bond donor functionalities (Figure 6b).

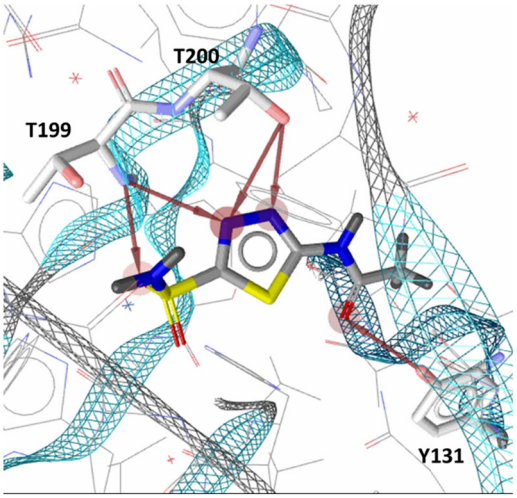

FIGURE 5 SB pharmacophore model generated from the X-ray crystal structure of acetazolamide (AAZ) in complex with murine CA V (PDB code: 1DMY).[32] The red arrows represent H-bond acceptor features.

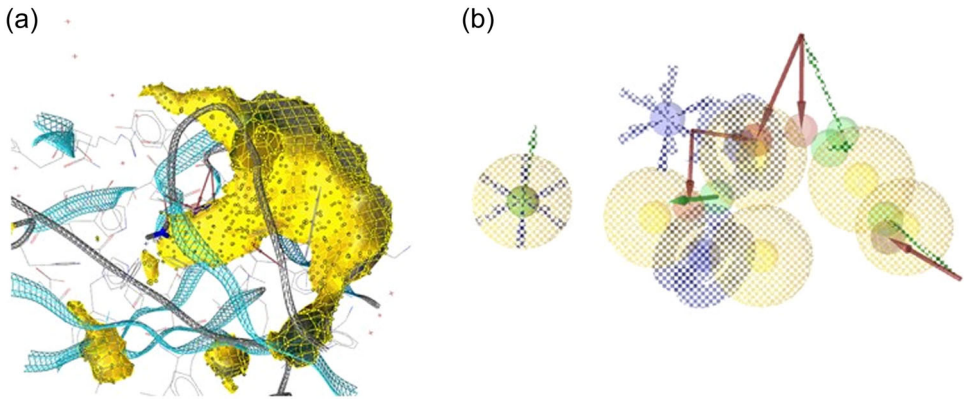

FIGURE 6 (a) Apo Site Grid generated starting from the X-ray crystal structure of acetazolamide (AAZ) in complex with CA V (PDB code: 1DMY). (b) The merged pharmacophore model: six hydrophobic spheres (light yellow spheres); two positive ionizable (blue star); two aromatic rings (blue circle); five H-bond acceptors (red arrows); five H-bond donors (green arrows). Optional features are not fully colored.

Based on the outcomes of the Apo Site analysis, the SB-based pharmacophore search filtered 38 molecules having a fit score value of more than 70. The list of the 38 selected compounds is reported in Supporting Information: Table S1.

2.2.2 | Docking studies

To preliminarily estimate the ability of the selected 38 molecules in interacting within the active site of the hCA V, we planned docking simulations. Since no X-ray data of hCA VA are available in literature, we tried to produce a homology model for hCA VA using TopModel server.[33] The quality of the model was assessed through TopScore, a meta Model Quality Assessment Program (meta-MQAP); it was found a value close to 0.1 (highest quality value) for the active site region. ProckectTool was used to trace Ramachandran plots, as result, 92.6% of the psi-phi angles lay inside favored regions and 7.4% are inside allowed or generously allowed regions (see Supporting Information: Figures S1 and S2). The model was minimized with Prime and used as a template for docking studies by Gold suite 5.0.1 with the CHEMPLP scoring function. Through this procedure, we selected 30 molecules displayed in Figures 7 and 8 and related docking score values are collected in Supporting Information: Table S2. All selected 30 ligands VAME-**01–30** share the common (hetero)arylsulfonamide moiety that is linked with distinct hydrophobic tails through a suitable linking moiety containing amine/amide/imine/thiourea chemical functionality.

Figure 9 displays the putative binding patterns of retrieved 30 molecules that were able to occupy the catalytic site of the modeled hCA VA. As expected, all compounds anchored the zinc-containing catalytic site through the sulfonamide moiety; moreover, they oriented the remaining molecular fragment within the two walls of the cavity. None of the selected sulfonamides possessed PAINS alerts as determined by the SwissADME platform (www.swissadme.ch).[34] Based on this predicted favorable recognition into hCA VA, the selected compounds were purchased from Specs supplier to determine their inhibitory effects on hCAs.

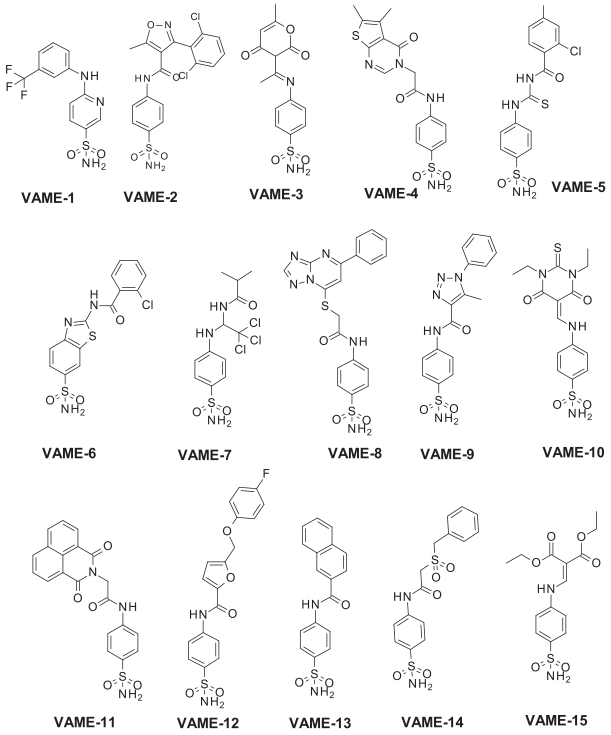

FIGURE 7 Chemical structures of the selected compounds VAME-**01–15**

2.3 | Evaluation of hCA inhibitory activity and selectivity

2.3.1 | In vitro studies

As mentioned in the previous section, the LB and SB screening of a focused Specs library generated the collection of 30 small molecules that were experimentally investigated as inhibitors against mitochondrial hCA VA isofom in comparison with ubiquitous and off-target hCA I-II isoforms. The K_i values of aminoarylsulfonamide-based compounds were

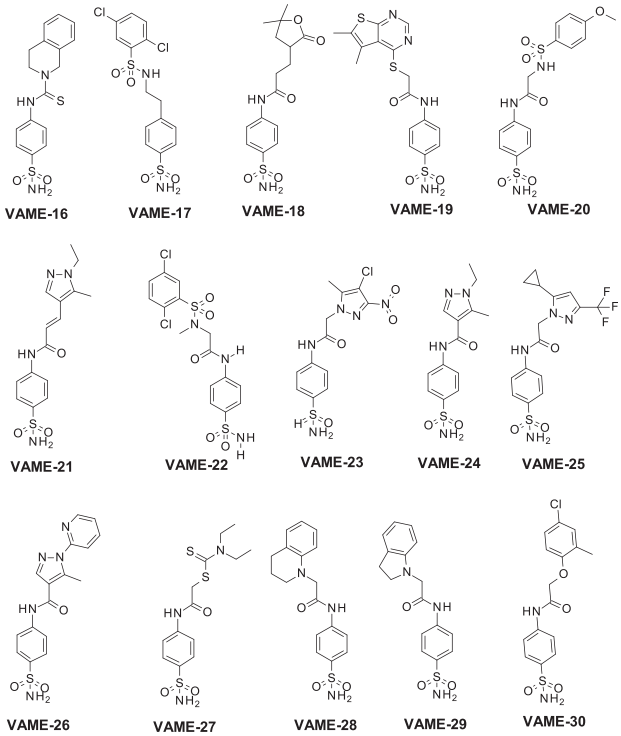

FIGURE 8 Chemical structures of the selected compounds VAME-**16–30**

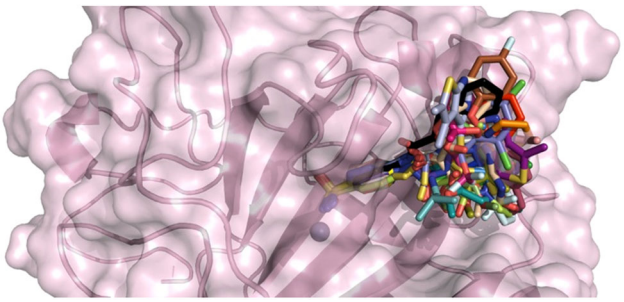

FIGURE 9 Putative binding poses of the 30 compounds, VAME-**01–30**, with the modeled human carbonic anhydrase (hCA) VA. The inhibitors are represented as colored sticks and the protein as a pink surface. Zinc ion is depicted as a gray sphere. Figure made by Pymol (https://pymol.org).

determined by using a stopped-flow CO_2 hydrase assay for evaluating their inhibitory potency. The resulting inhibition data are collected in Table 1 in comparison with reference compounds AAZ, TPM, and ZNS. As reported in Table 1, all 30 studied compounds were able to inhibit CO_2 hydration mediated by mitochondrial hCA VA demonstrating K_i values ranging from 33.4 to 794.4 nM concentration. Among the series, 19 compounds were endowed of inhibitory effects K_i values lower than 100 nM. Due to the presence of very nonhomogenous structural features of the molecular fragments linked to aminoarylsulfonamide moiety, a reliable structure-affinity relationship analysis was difficult to discuss; however, few considerations about the targeted hCA VA inhibition can be

TABLE 1 Inhibition data of tested sulfonamides and sulfamides VAME-**1–30** and reference compounds acetazolamide (AAZ), zonisamide (ZNS), and topiramate (TPM) and their selectivity ratios for the inhibition of human carbonic anhydrase (hCA) VA over the hCA I/hCA II isozymes

	K_i (nM)[a]			Sselectivity ratio	
Cmps	hCA I	hCA II	hCA VA	hCA I/ hCA VA	hCA II/ hCA VA
VAME-**01**	15.9	8.4	33.4	0.48	0.25
VAME-**02**	28.7	20	73.8	0.39	0.27
VAME-**03**	730.8	83.6	85.3	8.57	0.98
VAME-**04**	34.6	8.2	78.2	0.44	0.10
VAME-**05**	23.9	3.7	82.3	0.29	0.04
VAME-**06**	39.4	6	93.6	0.42	0.06
VAME-**07**	45.3	26.2	511.8	0.09	0.05
VAME-**08**	73.1	14.3	84.1	0.87	0.17
VAME-**09**	279.3	23.3	73.4	3.81	0.32
VAME-**10**	435.7	46.8	96.0	4.54	0.49
VAME-**11**	9.1	28.2	96.5	0.09	0.29
VAME-**12**	92.4	24.2	89.7	1.03	0.27
VAME-**13**	954	309.8	551.9	1.73	0.56
VAME-**14**	72	28.2	170.5	0.42	0.17
VAME-**15**	18.2	5.1	182.5	0.10	0.03
VAME-**16**	411.2	658.2	162.7	2.53	4.05
VAME-**17**	4.6	3.8	299.2	0.02	0.01
VAME-**18**	15.6	1.6	242.9	0.06	0.01
VAME-**19**	927.3	311.2	794.4	1.17	0.39
VAME-**20**	47.9	7.4	431.0	0.11	0.02
VAME-**21**	53.4	18.2	83.3	0.64	0.22
VAME-**22**	67.9	20.9	418.6	0.16	0.05
VAME-**23**	77.9	22.4	93.9	0.83	0.24
VAME-**24**	27.1	5.6	77.9	0.35	0.07
VAME-**25**	57.4	9.2	207.9	0.28	0.04
VAME-**26**	86.3	13.6	528.5	0.16	0.03
VAME-**27**	52.5	18.9	93.5	0.56	0.20
VAME-**28**	927.4	379.1	54.8	16.92	6.92
VAME-**29**	76.9	26.3	93	0.83	0.28
VAME-**30**	60.1	21.7	742.6	0.08	0.03
AAZ	250	12.1	63.0	3.97	0.19
ZNS[b]	56	35	20.0	2.80	1.75
TPM[b]	250	10	63.0	3.97	0.16

[a]Mean from three different assays. by a stopped-flow technique (errors were in the range of ±5%–10% of the reported values).
[b]Data taken from the literature.[27]

done based on data collected in Table 1. The best potent hCA VA inhibitors were the 6-[3-(trifluoromethyl)anilino]pyridine-3-sulfonamide (VAME-**01**, K_i value of 33.4 nM) and the 2-(3,4-dihydro-2H-quinolin-1-yl)-*N*-(4-sulfamoylphenyl)acetamide (VAME-**28**, K_i value of 54.8 nM) that resulted more potent than reference compounds AAZ (K_i value of 63.0 nM) and TPM (K_i value of 63.0 nM) and less active to respect to ZNS (K_i value of 20.0 nM). Notably, regarding the selectivity ratios over hCA I/hCA II isoforms (see Table 1), it might be observed that all studied compounds generally demonstrated poor selectivity over cytosolic hCA I and hCA II isoforms with exception of VAME-**28** bearing a 3,4-dihydroquinolinylacetamide tail linked to aminobenzenesulfonamide pharmacophore moiety. Notably, the active inhibitor VAME-**28** revealed a selective inhibition of hCA VA over hCA I/hCA II isoforms, thus demonstrating selectivity ratios of 16.92 and 6.92 for hCA I/hCA II, respectively. This selectivity profile is very enhanced when compared to reference compounds AAZ, TPM, and ZNS (see Table 1). Interestingly, for the analog compound 2-indolin-1-yl-*N*-(4-sulfamoylphenyl) acetamide (VAME-**29**) with indolyl system in place of quinolinyl one, the selectivity ratio significantly decreased (0.83 and 0.28 for hCA I and hCA II, respectively). These data confirmed that the hydrophobic tail could exert a crucial role in activity and/or selectivity toward hCAs.

2.3.2 | In silico analysis of hCA selectivity

To rationalize the high selectivity ratio over cytosolic hCA II for the active hCA VA inhibitor VAME-**28** and explain why a simple structural modification for VAME-**29** homolog significantly reduced the selectivity ratio over hCA II, we performed docking simulations. Figure 10 displays the putative binding site pattern of interaction of VAME-**28** with the modeled hCA VA in comparison with hCA II (PDB code 6XXT).[15] As you can see in Figure 10, VAME-**28** assumed two different binding poses when bound to hCA II or hCA VA. Even if the 4-aminobenzenesulfonamide moiety adopted a similar positioning close to the catalytic cavity of two proteins, the quinolinyl-tail assumed a very different binding orientation; this was presumably because the hCA VA had a broader hydrophobic binding area when compared with hCA II based on the very different orientation of crucial residue F131 (hCA II) (see Figure 10) corresponding to the Y129 in hCA VA. The above-mentioned different locations of aromatic residue F131 could push out VAME-**28** from the hydrophobic wall of hCA II cavity. On the contrary, the docked pose of VAME-**28** in hCA VA suggested an improved stabilization through interactions with the hydrophobic area lined by V133, Y129 as well as K130 (via alkyl-pi interaction); these data might contribute to explaining the about seven-folds improved affinity toward hCA VA (K_i value of 54.8 nM) to respect hCA II (K_i value of 379.1 nM).

The putative binding poses of VAME-**29** docked in hCA II and hCA VA are displayed in Figure 11. The docking simulations revealed that this inhibitor was able to accommodate the indolyl-tail toward the hydrophobic areas both of hCA II and hCA VA, where it potentially established favorable interaction with F131 and V135 of hCA II as well as Y129 and V133 of hCA VA. These data were coherent with the ability of compound VAME-**29** to exert inhibitory effects toward both hCA II and hCA VA.

Taken together these in silico results suggested that the steric hindrance brought by the replacement of five member-ring to a six-member one for the VAME-**28** inhibitor resulted in a very different

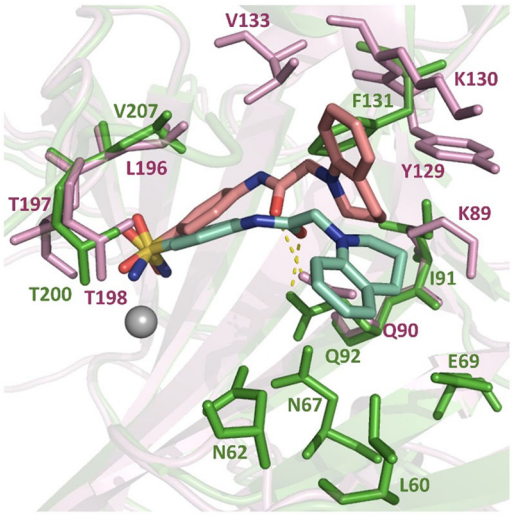

FIGURE 10 Superimposed binding modes of VAME-**28** bound to human carbonic anhydrase (hCA) VA (ligand as salmon stick and protein as a pink cartoon) and to hCA II (ligand as green-cyan stick and protein as a green cartoon). Interacting residues of hCA VA and hCA II are shown in pink and green, respectively. Hydrogen bonds are represented as yellow dashes. Zinc ion is depicted as a gray sphere. Figure made by Pymol.[35]

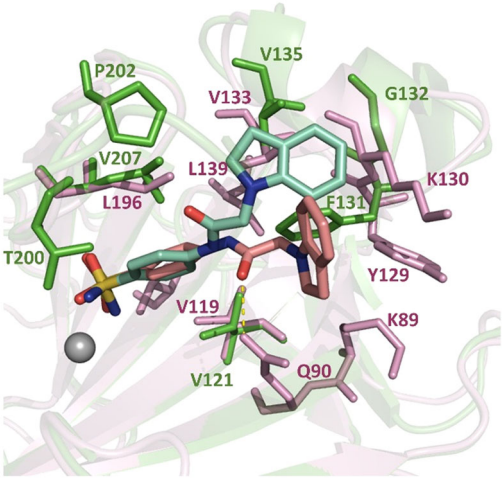

FIGURE 11 Superimposed binding modes of VAME-**29** bound to human carbonic anhydrase (hCA) VA (ligand as salmon stick and protein as a pink cartoon) and to hCA II (ligand as green-cyan stick and protein as a green cartoon). Interacting residues of hCA VA and hCA II are shown in pink and green, respectively. Hydrogen bonds are represented as yellow dashes. Zinc ion is depicted as a gray sphere. Figure made by Pymol.[35]

orientation in the top area of hCA cavity, thus exerting a fine-tuning in the isoform selectivity.

3 | CONCLUSION

In this study, we applied a workflow for making a VS on the Specs database of commercially available compounds with the aim of obtaining new inhibitors targeting hCA VA. First, we generated a LB pharmacophore model that provided a collection of hit compounds through VS. These compounds were docked in our modeled hCA VA and were experimentally tested by means of in vitro testing. Several compounds selected from these protocols were able to exert potent inhibition of hCA VA. The best outcome was the identification of a selective hCA VA inhibitor having a relevant selectivity ratio over ubiquitous cytosolic hCA I and hCA II. Based on these data, we analyzed the binding pose of the best compound, which represents a promising lead structure for further design ideas to identify selective and potent hCA VA for therapeutic purpose in obesity treatment.

4 | EXPERIMENTAL

4.1 | LB pharmacophore model generation

LigandScout V4.4.8[25] was used for the LB pharmacophore generation and the VS processes. All selected molecules (training set and test set) were constructed by Vega 3.2.2.[36] The pharmacophore model was generated using "merged features" option and the icon best mode has been used as the conformers generation method, the other parameters were left as default instead. The LB pharmacophore model was used as a template for searching against the SPECS database to find molecules that could potentially have an inhibitory effect. All VS runs were conducted by setting the option "Get best matching conformation" as retrieval mode and the obtained hits from screening were ranked based on their pharmacophore fit scores.

4.2 | SB pharmacophore model generation and VS

To create an SB pharmacophore model, the crystal complex between murine mitochondrial CA V and AAZ (PDB code 1DMY)[32] was used in LigandScout Suite.[25] To probe other plausible chemical features from the apo-structure of the protein, we generated the "apo-site" pharmacophore model taking into account only the buriedness surface, and setting the option "Append to existing pharmacophore." The following parameters were used for ApoSites generation: (i) Surface Grid = 0.25; (ii) Buriedness = 0.40; (iii) HBA Max = 7; (iv) HBD Max = 7; (v) Positive Ionizable Max = 7; (vi) Negative Ionizable Max = 7; (vii) Aromatic Max = 7; (viii) Hydrophobic Max = 7. The model was then refined marking as optional all the features except the features regarding the AZM zinc-chelator atoms. The obtained pharmacophore model was used as a template for the screening and molecules showing a pharmacophore fit-score value <70 were discarded.

4.3 | Homology modeling

The hCA V structure was modeled with TopModel,[37] using as main templates two different murine alpha-carbonic anhydrase V (PDB IDs: 1KEQ[38] and 1URT[39]) and the complex between murine mitochondrial CA V and the transition state analog AAZ (PDB ID: 1DMY).[32] The model was validated through measurement of the Topscore, which is a measure LDDT (local distance difference test) error, which indicates the uncertainty of the interatomic distances measured for a specific model. Low Topscore values reflect the high quality of the model. Hydrogens were added to the model through the server H++ (http://biophysics.cs.vt.edu/). The homology model built was then minimized through Prime software using OPLS3e applying restraint to the Zn atom and the zinc chelating histidines (H94, H96, and H119).

4.4 | Docking analysis

The obtained hCA V structure was used for docking studies of the 38 selected molecules. The ligands were minimized by Vega 3.2.2[36] using the Conjugate Gradient method (1000 steps) and were docked in the protein hCA V obtained by homology modeling, using Gold Suite 5.0.1[40] For the hCA V, the region of interest used by the Gold program was defined to contain the residues within 15 Å from the original position of the AAZ in the X-ray structure of the murine alpha-carbonic anhydrase V. CHEMPLP was chosen as the fitness function. The standard default settings were employed in all calculations. The ligands were submitted to 100 genetic algorithm runs. The "allow early termination" command was deactivated. The results were clustered together when differing by less than 0.75 Å in ligand-all atom RMSD. The highest GOLD fitness score was chosen for analysis and representation. The side chains of residues L65, Q92, V121, Y131, K132, V135, L141, L198, T199, and T200 were allowed to rotate in accordance with the internal rotamer libraries in GOLD Suite 5.0.1. For docking of VAME-**28** and VAME-**29** on hCA II, we used the 3D structure of 4-(4-aroylpiperazine-1-carbonyl) benzenesulfonamide derivative in complex with hCA II (PDB code 6XXT),[15] removing the ligand complexed and aligning the PDB structure 1DMY to it, removing murine CA VA structure, and saving the complex hCAII-AZM to sample the AZM coordinates for the docking. Sequence and Structural were used as alignment method on MOE and hydrogens were added through the same software using the Protonate 3D option and OPLS-AA forcefields, all the other settings were left as default. The same settings of the docking on CA VA were used on GOLD for the docking of the two derivatives on hCA II, using AZM centroids for defining the dockable region/binding site, sampling AZM coordinates as described before. The only difference between the two docking protocols here reported regards the side chains set as flexible in the first docking protocol, that in the latter case were left rigid. The molecular models of the docked ligands were displayed using Pymol software.[35]

4.5 | Determination of inhibitory effects against hCA I, hCA II, and hCA VA

The 30 compounds labeled VAME-**01–30** were bought from Specs (https://www.specs.net/) and used as such. The Specs database was chosen as a library of commercially available compounds for purchasing and testing. Based on the experiences of previous VS campaigns, this database contains molecules having a certain chemical diversity combined with good purity and availability. In detail, the purity of the compound reported by the manufacturer was greater than 95%. For each compound, the Specs ID number is reported in Supporting Information: Table S1. Moreover, the InChI codes of the collection of 30 investigated compounds VAME-**01–30**, together with biological activity data, are provided as supporting material. The CA inhibition assay was performed by using a stopped-flow CO_2 hydration assay[41] as previously described.[18,19,30]

ACKNOWLEDGMENTS

The authors thank Ester D'Agostino for her contribution to the modeling section. This study was financially supported by a grant (PRIN_201744BN5T_002) from the Italian Ministry of University and Research (MUR). Open Access Funding provided by Universita degli Studi di Messina within the CRUI-CARE Agreement.

CONFLICTS OF INTEREST

The authors declare no conflicts of interest.

ORCID

Laura De Luca http://orcid.org/0000-0003-0614-5713

Rosaria Gitto http://orcid.org/0000-0003-0002-2253

REFERENCES

[1] Y. J. Tak, S. Y. Lee, *Curr. Obes. Rep.* **2021**, *10*, 14.
[2] A. Cignarella, L. Busetto, R. Vettor, *Pharmacol. Res.* **2021**, *169*, 105649.
[3] E. Pilitsi, O. M. Farr, S. A. Polyzos, N. Perakakis, E. Nolen-Doerr, A. E. Papathanasiou, C. S. Mantzoros, *Metabolism* **2019**, *92*, 170.
[4] R. Khera, M. H. Murad, A. K. Chandar, P. S. Dulai, Z. Wang, L. J. Prokop, R. Loomba, M. Camilleri, S. Singh, *JAMA* **2016**, *315*, 2424.
[5] T. D. Muller, M. Bluher, M. H. Tschop, R. D. DiMarchi, *Nat. Rev. Drug. Discov.* **2021**, *21*, 201.
[6] C. T. Supuran, *Expert Opin. Drug Metab. Toxicol.* **2020**, *16*, 297.
[7] C. T. Supuran, C. Capasso, *Int. J. Mol. Sci.* **2021**, *22*, 4324.
[8] A. Scozzafava, C. T. Supuran, F. Carta, *Expert Opin. Ther. Pat.* **2013**, *23*, 725.
[9] C. T. Supuran, *J. Enzyme Inhib. Med. Chem.* **2021**, *36*, 1702.
[10] S. Kumar, S. Rulhania, S. Jaswal, V. Monga, *Eur. J. Med. Chem.* **2021**, *209*, 112923.
[11] N. Y. Khalil, H. K. AlRabiah, S. S. Al Rashoud, A. Bari, T. A. Wani, *Profiles Drug Subst. Excip. Relat. Methodol.* **2019**, *44*, 333.
[12] Q. Shi, Y. Wang, Q. Hao, P. O. Vandvik, G. Guyatt, J. Li, Z. Chen, S. Xu, Y. Shen, L. Ge, F. Sun, L. Li, J. Yu, K. Nong, X. Zou, S. Zhu, C. Wang, S. Zhang, Z. Qiao, Z. Jian, Y. Li, X. Zhang, K. Chen, F. Qu, Y. Wu, Y. He, H. Tian, S. Li, *Lancet* **2021**, *399*, 259.
[13] K. Fujioka, *Diabetes. Obes. Metab.* **2015**, *17*, 1021.
[14] F. Mancuso, A. Di Fiore, L. De Luca, A. Angeli, G. De Simone, C. T. Supuran, R. Gitto, *Bioorg. Med. Chem.* **2021**, *44*, 116279.
[15] F. Mancuso, A. Di Fiore, L. De Luca, A. Angeli, S. M. Monti, G. De Simone, C. T. Supuran, R. Gitto, *ACS Med. Chem. Lett.* **2020**, *11*, 1000.
[16] M. R. Buemi, A. Di Fiore, L. De Luca, A. Angeli, F. Mancuso, S. Ferro, S. M. Monti, M. Buonanno, E. Russo, G. De Sarro, G. De Simone, C. T. Supuran, R. Gitto, *Eur. J. Med. Chem.* **2019**, *163*, 443.
[17] R. Gitto, F. M. Damiano, P. Mader, L. De Luca, S. Ferro, C. T. Supuran, D. Vullo, J. Brynda, P. Rezacova, A. Chimirri, *J. Med. Chem.* **2012**, *55*, 3891.
[18] P. Mader, J. Brynda, R. Gitto, S. Agnello, P. Pachl, C. T. Supuran, A. Chimirri, P. Rezacova, *J. Med. Chem.* **2011**, *54*, 2522.
[19] R. Gitto, S. Agnello, S. Ferro, L. De Luca, D. Vullo, J. Brynda, P. Mader, C. T. Supuran, A. Chimirri, *J. Med. Chem.* **2010**, *53*, 2401.
[20] C. T. Supuran, *Expert Opin. Drug Discov.* **2020**, *15*, 671.
[21] A. Nocentini, C. T. Supuran, *Expert Opin. Drug Discov.* **2019**, *14*, 1175.
[22] D. Idrees, M. Shahbaaz, K. Bisetty, A. Islam, F. Ahmad, M. I. Hassan, *J. Biomol. Struct. Dyn.* **2017**, *35*, 449.
[23] G. Costa, A. Artese, F. Ortuso, S. Alcaro, *Methods Mol. Biol.* **2021**, *2266*, 263.
[24] G. Costa, F. Carta, F. A. Ambrosio, A. Artese, F. Ortuso, F. Moraca, R. Rocca, I. Romeo, A. Lupia, A. Maruca, D. Bagetta, R. Catalano, D. Vullo, S. Alcaro, C. T. Supuran, *Eur. J. Med. Chem.* **2019**, *181*, 111565.
[25] G. Wolber, T. Langer, *J. Chem. Inf. Model.* **2005**, *45*, 160.
[26] F. Z. Smaine, F. Pacchiano, M. Rami, V. Barragan-Montero, D. Vullo, A. Scozzafava, J. Y. Winum, C. T. Supuran, *Bioorg. Med. Chem. Lett.* **2008**, *18*, 6332.
[27] O. Guzel, A. Innocenti, A. Scozzafava, A. Salman, C. T. Supuran, *Bioorg. Med. Chem.* **2009**, *17*, 4894.
[28] S. A. Poulsen, B. L. Wilkinson, A. Innocenti, D. Vullo, C. T. Supuran, *Bioorg. Med. Chem. Lett.* **2008**, *18*, 4624.
[29] A. Cecchi, S. D. Taylor, Y. Liu, B. Hill, D. Vullo, A. Scozzafava, C. T. Supuran, *Bioorg. Med. Chem. Lett.* **2005**, *15*, 5192.
[30] J. Y. Winum, A. Thiry, K. E. Cheikh, J. M. Dogne, J. L. Montero, D. Vullo, A. Scozzafava, B. Masereel, C. T. Supuran, *Bioorg. Med. Chem. Lett.* **2007**, *17*, 2685.
[31] D. Vullo, M. Franchi, E. Gallori, J. Antel, A. Scozzafava, C. T. Supuran, *J. Med. Chem.* **2004**, *47*, 1272.
[32] P. A. Boriack-Sjodin, R. W. Heck, P. J. Laipis, D. N. Silverman, D. W. Christianson, *Proc. Natl. Acad. Sci. U.S.A.* **1995**, *92*, 10949.
[33] D. Mulnaes, F. Koenig, H. Gohlke, *J. Chem. Inf. Model.* **2021**, *61*, 548.
[34] A. Daina, O. Michielin, V. Zoete, *Sci. Rep.* **2017**, *7*, 42717.
[35] The PyMOL Molecular Graphics System, Version 2.0, Schrödinger, LLC.
[36] A. Pedretti, L. Villa, G. Vistoli, *J. Mol. Graph. Model.* **2002**, *21*, 47.
[37] D. Mulnaes, N. Porta, R. Clemens, I. Apanasenko, J. Reiners, L. Gremer, P. Neudecker, S. H. J. Smits, H. Gohlke, *J. Chem. Theory Comput.* **2020**, *16*, 1953.
[38] K. M. Jude, S. K. Wright, C. Tu, D. N. Silverman, R. E. Viola, D. W. Christianson, *Biochemistry* **2002**, *41*, 2485.
[39] R. W. Heck, P. A. Boriack-Sjodin, M. Qian, C. Tu, D. W. Christianson, P. J. Laipis, D. N. Silverman, *Biochemistry* **1996**, *35*, 11605.
[40] G. Jones, P. Willett, R. C. Glen, A. R. Leach, R. Taylor, *J. Mol. Biol.* **1997**, *267*, 727.
[41] R. G. Khalifah, *J. Biol. Chem.* **1971**, *246*, 2561.

SUPPORTING INFORMATION

Additional supporting information can be found online in the Supporting Information section at the end of this article.

How to cite this article: L. De Luca, A. Angeli, F. Ricci, C. T. Supuran, R. Gitto, *Arch. Pharm.* **2023**;356:e2200383. https://doi.org/10.1002/ardp.202200383